Characterization of mercury gilding art objects by external proton beam

V. Corregidor [a,b,*], L.C. Alves [a,b], N.P. Barradas [a,b], M.A. Reis [a,c], M.T. Marques [d,e], J.A. Ribeiro [d,e]

[a] Unidade de Física e Aceleradores, LFI, ITN, E.N.10, 2686-953 Sacavém, Portugal
[b] CFNUL, Av. Prof. Gama Pinto, 2 1649-003 Lisboa, Portugal
[c] CFAUL, Av. Prof. Gama Pinto, 2 1649-003 Lisboa, Portugal
[d] Casa-Museu Dr. Anastácio Gonçalves, Av. 5 de Outubro, 6-8 1050-055 Lisboa, Portugal
[e] IMC, Palácio Nacional da Ajuda, 1349-021 Lisboa, Portugal

ARTICLE INFO

ABSTRACT

The fire gilding is one of the methods used by the ancient goldsmiths to obtain a rich, metallic glow and durable golden appearance in ornamental objects. This layer is characterized, among others, by its thickness (several microns) a diffusion profile and a Hg content (between 0 and 21 wt.%) depending on the temperatures achieved during the process. Gilded sacral art objects dated from the XVI to the XVIII centuries, belonging to the Casa-Museu Dr. Anastácio Gonçalves Collection (Lisbon) were analyzed using the external ion microprobe at Nuclear and Technological Institute, Lisbon. The average concentrations of the homogeneous areas were calculated with GUPIX, DATTPIXE and NDF codes showing very similar results. The RBS and PIXE spectra from the same point were collected simultaneously and analyzed together with NDF-LibCPIXE in order to find self-consistent solutions. Profile concentration on particular Au-reach points was extracted. Different Hg and Au/Ag ratio have been found in the pieces dating from different centuries.

1. Introduction

The application of a gold coating onto the surface of a lower quality alloy to make an object look like cast gold has been widely used since ancient times. This method, known as gilding, also improves the corrosion resistance of the objects. The gilding has evolved during years, following the requirements of the finals users (price, quality) and taking advantage of the technological advances along the years, such as the development of methods for the purification of gold or improvements of surface treatment. During circa the third millennium BC, gilded objects were produced by covering them with a gold foil and lately attached mechanically [1]. Around the first century BC, gold leafs were attached to the surface with organic adhesive, e.g. egg or animal glue [2], and some centuries later the fire-gilding (also known as mercury-gilding) became widespread used, as described by Theophilus in the twelfth century [3]. The best workshops around the mid-end eighteenth century were located in France due to the richness and refinement in the finish look of the objects [1,4]. In South America, the goldsmiths used the so called depletion gilding method, where from a gold–copper alloy usually with a very low gold content

(known as the "tumbaga" alloy) and an appropriate surface chemical treatment, the result was a gold enriched surface, making the tumbaga jewellery look like pure gold [5,6]. Nowadays, all these techniques have been replaced by others, for example electroplating.

Nowadays there is a general consensus about the need of conservation and restoration of the Cultural Heritage objects. Definition of the proper conservation and restoration procedures requires the knowledge, among others, of composition, provenance region of the raw materials, manufacturing technique, etc.

There are several techniques available to study the composition of objects, but some of them have disadvantages when applied to Cultural Heritage objects. The IBA (Ion Beam Analysis) techniques allow the determination of elemental composition, distribution and depth profile in these objects in a non-destructive way. Furthermore, when these techniques are implemented at atmospheric pressure using an external ion beam, the number of applications becomes wider since sampling is not needed, the size of the objects is not crucial and some fine art objects, which cannot be put under vacuum, can be studied. Several research works can be found in the literature about the IBA techniques applied to the study of metal objects [2,6–9]. Among the IBA techniques, Particle Induced X-ray Emission (PIXE) and Rutherford Backscattering Spectroscopy (RBS) are the most commonly used in the analysis of cultural heritage objects, being complementary. From the analysis of RBS spectra, surface composition and elemental depth profile of the different elements can be extracted but the mass resolution in

* Corresponding author at: Unidade de Física e Aceleradores, LFI, ITN, E.N.10, 2686-953 Sacavém, Portugal. Tel.: +351 219946080; fax: +351 219941525.
E-mail addresses: vicky.corregidor@itn.pt (V. Corregidor), lcalves@itn.pt (L.C. Alves), nunoni@itn.pt (N.P. Barradas), mareis@itn.pt (M.A. Reis), cmag.teodoramarques@imc-ip.pt (M.T. Marques), cmag@imc-ip.pt (J.A. Ribeiro).

certain experimental conditions (the use of proton beam, elements with close atomic numbers) can be degraded. On the other hand PIXE has a high sensitivity, ideal to study trace elements, but the extraction of information related to the depth profile of the elements is not straightforward.

Gilded sacred art objects dated from the XVI to the XVIII centuries, belonging to the Casa-Museu Dr. Anastácio Gonçalves (CMAG) Collection (Lisbon) were analyzed using the external ion microprobe at Nuclear and Technological Institute, Lisbon (Portugal). In this paper, we present the first results obtained with this set-up applied to metallic objects coming from the Museum collection.

2. Experimental method

2.1. Objects

Three objects belonging to the CMAG Collection of sacred art were chosen to perform this work. The reliquary (CMAG 1194) from the XVI century has two visible hallmarks (AR SII) on the base and on the lid, and it is believed to be of Spanish origin. The ostensorium (CMAG 1164) from the mid-XVIII century has a visible hallmark, indicating the goldsmith (J.P./C.) and the Portuguese origin (a crown L, from Lisbon). The Ciborium (CMAG 1180) has an oval base, and it is partially gilt, with several religious motifs.

The three pieces are gilded and, according with their different provenances and manufacturing date, differences in composition between them are expected.

2.2. Experimental

For the analysis by PIXE and RBS no special surface preparation was done. As the objects are in exhibition at the CMAG, the conservation state is optimum and no soil contaminant trace elements were expected. No restoration processes on the objects are recorded. After the measurements no visible marks were observed on the surfaces.

During the experiments the RBS and PIXE spectra were recorded simultaneously using the external microprobe [10], at the 2.5 MV single ended Van de Graaff accelerator at ITN [11].

The 2 MeV proton beam is extracted from the vacuum beam line through a 100 nm thick Si_3N_4 membrane on a 200 μm thick Si frame with a 1 mm^2 window and focussed to a final spot of 60 μm diameter, with a final energy of 1940 keV and with a intensity of 200 pA. External scans as large as 800×800 μm^2 can be performed. The distance between the exit window and the sample is 3 mm, controlled by the intersection of two laser beams observed with a micro-camera connected to a computer. The beam incidence is normal to the target surface and two detectors are placed in the IBM geometry. The X-ray detector is a Si Bruker SDD detector with an active area of 30 mm^2, 8 μm Be window and 145 eV resolution at 5.9 keV placed at 2.8 cm from the sample at an angle of 45° to the beam direction. The backscattered particles are detected with a surface barrier detector placed at 133° scattering angle and 2.2 cm from the sample. A controlled Helium flow is used during the experiments to reduce proton energy loss and straggling then improving the beam spatial resolution and also contributing to reduce X-ray attenuation.

Although some X-ray spectra were acquired without using any filter in front of the X-ray detector, most of them were obtained with a 350 μm thick Mylar foil in order to filter the Au and Hg M-lines. Layered target information was gathered through the recorded RBS spectra. For the data analysis different computer codes were used. For PIXE spectra GUPIX [12], QXAS [13] and DATTPIXE [14] codes were applied to extract the elemental concentration or peak areas, according with the code. The NDF code [15] was used

for RBS spectra fitting and sample composition determined in a self-consisting way with PIXE data simulated by means of LibCPIXE code [16], an open-source library for multilayered samples which can work jointly with the NDF code. When non-Rutherford cross sections were needed, they were calculated using SigmaCal [17]. The suitability of the codes for the study of the objects presented in this work will be discussed in the next section.

Two reference samples with well-known composition, brass NBS 1105 and Ag–Cu (80–20) alloy, were analyzed throughout the measurements. The data were used to attain the relative efficiency curve of the system (detector + "air" path + filter).

3. Results and discussion

A photograph of the experimental setup is shown in Fig. 1, where the proton beam is hitting an edge on the reliquary base.

For comparison of the elemental concentrations obtained with the three codes previously referred, a flat surface with no ornamentation and larger than the beam size was chosen, in order to assure the proper orientation of the irradiated surface with respect to the direction of the incident beam and the position of the detectors. The precise area for the analysis showed a homogeneous composition in the 2D PIXE maps (800×800 μm^2).

The X-ray spectrum recorded in one of these areas is shown in Fig. 2. The fit obtained using GUPIX is also shown in Fig. 2 and the concentration values are presented in Table 1. Also in Table 1 the data obtained when using DATTPIXE and NDF are given. The net peak area needed for these two codes were obtained with the QXAS program. In all cases two filters were considered for the quantitative analysis, corresponding to the air distance between the sample–detector and the 350 μm Mylar foil.

The codes give slightly different results, with the major elements presenting maximum relative deviation of 4% for Ag, 3% for Au and 3% for Hg. The differences found should be related not only to the diverse databases and algorithms used in the calculation of sample X-ray yields but also to the spectrum deconvolution procedure used on each software code, in particular when defining detector and spectra background parameters.

The average thickness of a gold layer formed by the fire-gilding method is large (several microns) and there is a wide (about 10 μm) interdiffusion region into the substrate [18,19]. Protons with 1940 keV energy used during these measurements have a penetration depth close to 14 μm, so the results presented in this work are restricted to the first microns of the surface and depending on the object or area analyzed we are able to characterize the

Fig. 1. Experimental setup at ITN, with the reliquary (CMAG 1194 Collection) placed in front of the external beam (3 mm distance) before the analysis; (1) X-ray detector with Mylar foil; (2) micro-camera; (3) beam exit nozzle with 100 nm Si_3N_4 window; (4) RBS detector with He flow.
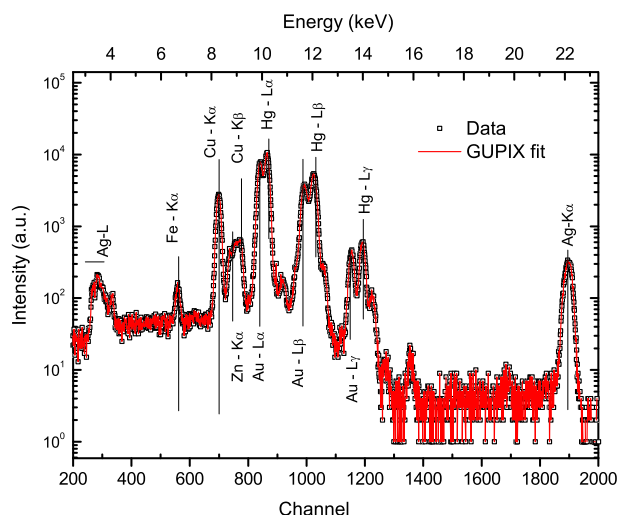
Fig. 2. PIXE spectrum and GUPIX fit from a homogeneous composition area. Object: Reliquary (CMAG 1194 Collection).

beginning of the diffusion region, while clear information from the core of the object can not be extracted. Because of that, the concentration values presented here are referred to areas with a homogeneous composition and for the calculus only one layer was considered. According with the previous discussion, DATTPIXE was used.

The ciborium external surface has a white silvery aspect, with many decoration designs, some of them gilded. The inside of the cup and the cover, following the Ecclesiastical directives, are completely gilt. The analysis performed on the internal part of the cover show an average composition of 25% of Ag, 60% of Au and 15% of Hg, with a homogeneous distribution of the elements. The inner side of the cup could not be characterized due to geometrical set-up issues.

Some of the external white silvery parts were analyzed and in all cases traces of Hg were found. The Hg concentration depends on how close we measure to a gilded area. Concentrations up to 2% can be found a few millimeters from a gilded area and 0.1% of Hg is measured in a far away part. On the other hand, traces of Au are also found in these areas with a nearly constant composition (between 0.2% and 0.3%).

This Au and Hg contamination can be related with the gilding process, the atoms from the vapors (most of them mercury) [18] formed during the heating step in a particular area can be deposited on a cooler surface, and absorbed into the silver because of the very high solid solubility of mercury in silver.

The external gilded areas of the ciborium have a much lower Hg content (in the range of 5–7%) when compared with the internal cover and the ratio of Ag/Au is also different. This behavior is due to the gilding process as the final composition depends on the duration of the heating and temperature reached [18].

In Figs. 3 and 2D maps of the X-ray emission lines for four elements (Ag, Cu, Hg and Au) obtained from the base of the ciborium are shown. The RBS spectrum simultaneously recorded is shown in Fig. 4a. Some regions with dimensions up to 85 μm with inhomogeneous composition can be identified. Point analysis on one of these regions was done and the corresponding RBS spectrum is also shown in Fig. 4b. In this case, from the RBS spectrum we have enough sensibility to resolve the depth composition assuming a multilayer structure with a gradient composition. As both GUPIX and DATTPIXE can perform multilayer analysis only if each of the selected elements belongs to one and only one definite layer, they cannot be applied in this case. Instead NDF was used, considering a first layer with a mixture of Au and Ag as principal elements and then a diffusion region of Au into the silver. The comparison between the experimental and fitted data from the main X-ray lines of the elements are shown in Fig. 4c. For silver concentration calculation, the Ag–K emission line emission was considered. The composition calculated for the profile for this point analysis and for the average area of the scan can be found in Table 2.

The monstrance of the ostensorium is made of silver. The analyses performed did not indicate the presence of Au or Hg, as in the case of the ciborium. The ostensorium comprises several parts attached by screws and can be dismantled. The gilding processes of the base, knob and stem were made separately and then mounted, giving no chance of Au or Hg contamination. The rays surrounding the monstrance have a dull yellow appearance and
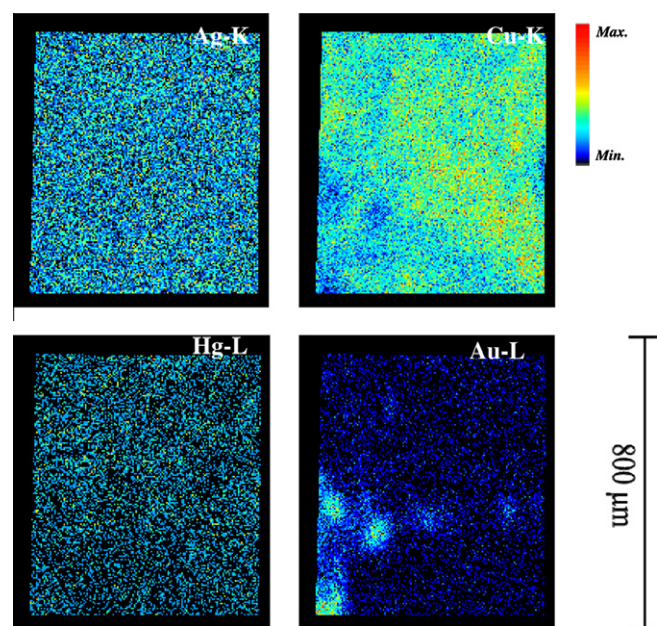

Fig. 3. 800 × 800 μm² PIXE maps for Ag, Cu, Hg and Au elements. Data obtained from an area of the base of the Ciborium (CMAG 1180).

Table 1
Concentrations values (wt.%) obtained with GUPIX, DATTPIXE and NDF-LibCPIXE codes extracted from the X-ray spectrum shown in Fig. 2. The digit in parentheses is the one affected by the estimated error of the calculated concentration. The relative error was estimated to be of 2% for the major elements, 5% for the minor components and 10% for trace elements whenever these values are superior to the errors due to counting statistics and spectra fitting. (N.d., not detected).

| Code	Concentration (wt.%)									
	Ca	Fe	Ni	Cu	Zn	Ag	Au	Hg	Pb	Bi
GUPIX	0.06(2)	0.04(8)	N.d.	1.4(9)	0.04(8)	47.(5)	20.(6)	30.(0)	0.1(4)	N.d.
DATTPIXE	0.09(4)	0.05(5)	N.d.	1.6(3)	0.02(0)	47.(8)	21.(2)	28.(9)	0.2(8)	0.04(1)
WiNDF	0.1(3)	0.05(9)	N.d.	1.7(8)	0.02(1)	45.(9)	21.(7)	30.(1)	0.2(7)	N.d.
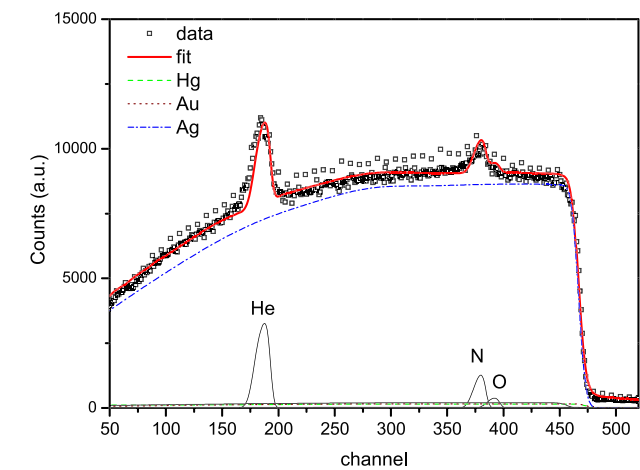
Fig. 4a. RBS spectrum, fit and partial spectra for each element corresponding to the overall area shown in Fig. 3. Signals from elements with a low concentration are not shown.
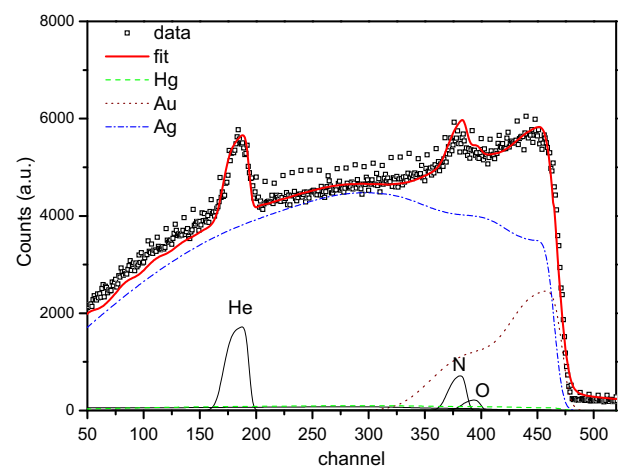
Fig. 4b. RBS spectrum, fit and partial spectra for each element from a point measurement with higher concentration of gold. Signals from elements with a low concentration are not shown.
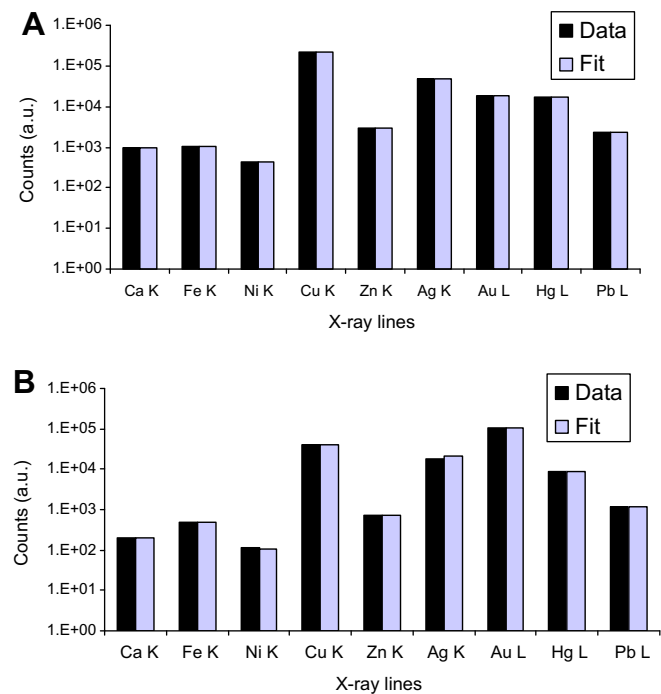
Fig. 4c. Experimental peak net area data for the main X-ray lines of the considered elements and simulation data derived from the attained sample composition during the fit. (A) Data from the overall scanned sample area; (B) Data from point analysis on Au most intense region shown in the maps of Fig. 3.

it was not possible to detect Hg. They are made of an Ag–Au–Cu alloy with concentration of 85%, 12% and 3%, respectively.

Generally speaking, and comparing the composition extracted for several points on two of the pieces which are totally gilded, the ostensorium has an average Hg content (12%) which is larger than the one observed for the reliquary (10%). About two centuries separate the goldsmiths responsible for these objects and probably different production locations and sources of the materials explain the differences between them.

4. Conclusions

When a homogeneous area of analysis is considered, the average composition obtained with the GUPIX, DATTPIXE and NDF codes is quite similar, even though improvements should be pursued especially in what accounts to Ag–Hg concentration. Efforts related with finer detector efficiency calibration, stability of the He flow control and data base consistency issues should be done to overcome the registered differences.

In some particular cases the simultaneous fitting of the RBS and the PIXE experimental data reveals that the inhomogeneous composition observed in the PIXE maps are mainly due to superficial inclusions which are Au rich with a diffusion profile into the silver object.

Different Hg and Au/Ag ratio have been found in the reliquary and ostensorium pieces dating from different centuries and provenances. In the silvery parts of the ciborium, which is partially fire-gilded, some traces of Hg and Au were found, related with the manufacture process.

Table 2
Concentration values (wt.%) obtained with NDF-LibCPIXE code corresponding: (a) average composition of the area shown in Fig. 3; (b) profile concentration in one of the Au-rich areas shown in Fig. 3. (N.d., not detected).

	Concentration (wt.%)								
	Ca	Fe	Ni	Cu	Zn	Ag	Au	Hg	Pb
(a)									
	0.18	0.02	0.01	3.38	0.05	93.99	1.14	1.07	0.16
(b)									
1st layer 5394×10^{15} at/cm^2	0.08	0.01	N.d.	0.25	0.02	67.58	31.20	0.71	0.15
2nd layer 8367×10^{15} at/cm^2	0.15	0.02	N.d.	1.34	0.03	80.99	16.29	1.02	0.16
3rd layer substrate	0.23	0.03	0.01	2.52	0.03	95.65	0.00	1.35	0.18

The external set-up at ITN is currently under improvement to allow the confident measurement of the beam current and the total charge deposited during the experiment. In a near future a second X-ray detector will allow the simultaneous record of the low and medium-high energy regions of the X-ray sample spectrum at the same time, reducing the time the beam is hitting the surface of the object.

Acknowledgement

References

[1] A. Oddy, Gold Bull. 14 (1981) 75.
[2] M.F. Guerra, T. Calligaro, Meas. Sci. Technol. 14 (2003) 1527.
[3] J.G. Hawthorne, C.S. Smith, On Divers Arts: The Treatise of Theophilus, The Chicago University Press, 1963, pp. 112 (Reprinted Dover New York 1979).
[4] M. Chapman, in: D.A. Scott, J. Podany, B.B. Considine (Eds.), Ancient and Historic Metals, Getty Conservation Institute, 1991, pp. 229.
[5] W. Bray, Gold. Bull. 11 (1978) 136.
[6] G. Demortier, J.L. Ruvalcaba-Sil, Nucl. Instr. and Meth. B 239 (2005) 1.
[7] A. Perea, A. Climent-Font, M. Fernández-Jiménez, O. Enguita, P.C. Gutiérrez, S. Calusi, A. Migliori, I. Montero, Nucl. Instr. and Meth. B 249 (2006) 638.
[8] M.D. Ynsa, J. Chamón, P.C. Gutiérrez, I. Gomez-Morilla, O. Enguita, A.I. Pardo, M. Arroyo, J. Barrio, M. Ferretti, A. Climent-Fong, Appl. Phys. A 92 (2008) 235.
[9] R. Borges, I. Tissot, A.I. Seruya, R.J.C. Silva, S. Fragoso, B. Maduro, A. Pais, X-ray Spectrom. 37 (2008) 338.
[10] L.C. Alves, P.A. Rodrigues, M. Vilarigues, R.C. da Silva, in: Proc. 10th International Conference on Nuclear Microprobe Technology and Applications, 2006, <http://www.itn.pt/projs/microfex/PIXE2007.jpg>.
[11] L.C. Alves, M.B.H. Breese, E. Alves, A. Paúl, M.R. da Silva, M.F. da Silva, J.C. Soares, Nucl. Instr. and Meth. B 161–163 (2000) 334.
[12] J.A. Maxwell, W.J. Teesdale, J.L. Campbell, Nucl. Instr. and Meth. B 95 (1995) 407.
[13] QXAS Seibersdorf Laboratories, IAEA, <http://www.iaea.or.at/programmes/ripc/physics/faznic/qxas.htm>.
[14] M.A. Reis, L.C. Alves, Nucl. Instr. and Meth. B 95 (1992) 300.
[15] N.P. Barradas, C. Jeynes, K.P. Homewood, B.J. Sealy, M. Milosavljevic, Nucl. Instr. and Meth. B 139 (1998) 235.
[16] C. Pascual-Izarra, N.P. Barradas, M.A. Reis, Nucl. Instr. and Meth. B 249 (2006) 820.
[17] A.F. Gurbich, Nucl. Instr. and Meth. B 268 (2010) 1703, <http://www-nds.iaea.org/sigmacalc/>.
[18] K. Anheuser, Met. Mater. Soc. 49 (1997) 58.
[19] J. Salomon, J.C. Dran, T. Guillou, B. Moignard, L. Pichon, P. Walter, F. Mathis, Appl. Phys. A 92 (2008) 43.